NANO LETTERS

pubs.acs.org/NanoLett Letter

Emerging Magnetic Interactions in van der Waals Heterostructures

Yulong Huang, Christian Wolowiec, Taishan Zhu, Yong Hu, Lu An, Zheng Li, Jeffrey C. Grossman, Ivan K. Schuller, and Shenqiang Ren*

Cite This: *Nano Lett.* 2020, 20, 7852−7859 Read Online

ACCESS | Metrics & More | Article Recommendations | Supporting Information

ABSTRACT: Vertical van der Waals (vdWs) heterostructures based on layered materials are attracting interest as a new class of quantum materials, where interfacial charge-transfer coupling can give rise to fascinating strongly correlated phenomena. Transition metal chalcogenides are a particularly exciting material family, including ferromagnetic semiconductors, multiferroics, and superconductors. Here, we report the growth of an organic−inorganic heterostructure by intercalating molecular electron donating bis(ethylenedithio)tetrathiafulvalene into (Li,Fe)OHFeSe, a layered material in which the superconducting ground state results from the intercalation of hydroxide layer. Molecular intercalation in this heterostructure induces a transformation from a paramagnetic to spin-glass-like state that is sensitive to the stoichiometry of molecular donor and an applied magnetic field. Besides, electron-donating molecules reduce the electrical resistivity in the heterostructure and modify its response to laser illumination. This hybrid heterostructure provides a promising platform to study emerging magnetic and electronic behaviors in strongly correlated layered materials.

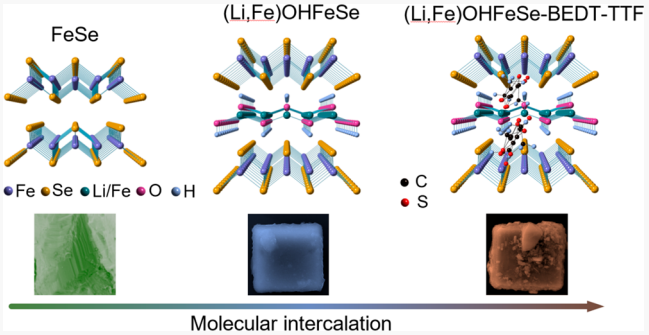

KEYWORDS: *van der Waals heterostructure, charge transfer, molecular intercalation, magnetism*

The structural engineering of quantum materials has attracted much research interest with attention focused on the exploration of electronic and magnetic properties, increasing an understanding of underlying physical mechanisms, and creating a pathway for potential applications in energy, quantum sensing, and communication.[1−4] In this context, chemical doping, extreme pressure, epitaxial strain, and electric gating have been utilized to control the electronic and spin structure of quantum materials to uncover emerging phenomena such as superconductivity, topological phases, and magnetic orders.[5−11] The vdWs heterostructures are excellent candidates to explore quantum tuning based on their intrinsic interfacial coupling and interactions.[12−19]

The structural engineering of iron selenide (FeSe)-based superconductors, through metal doping, molecular intercalation, application of high pressure, and interfacial strain, has yielded various results which are characterized by richly correlated phenomena.[20−24] The highest superconducting critical temperature (T_c) of FeSe-based superconductors has reached 65 K, and in one case above 100 K,[25,26] in which superconductivity was realized at the interface of a one-unit-cell film of FeSe on a $SrTiO_3$ substrate. Numerous FeSe-based derivative materials that are electron-doped with alkalis or molecules have suggested a tremendous flexibility in materials by design.[27−29] (Li,Fe)OHFeSe (LFS) layered material is representative of a molecule intercalated system in which a charge-transfer interface may enhance superconductivity with a higher T_c compared to that of binary FeSe.[28,30] Electron-donating bis(ethylenedithio)tetrathiafulvalene (BEDT-TTF, abbreviated as ET) salts are known for their role in molecular superconductors, Mott insulators, and quantum spin liquids.[31−38] Generally, two ET molecules in a strongly correlated system are dimerized face-to-face and form a conducting layer where each dimer is a hole site with an unpaired spin, like κ-$(BEDT\text{-}TTF)_2Cu[N(CN)_2]Cl$.[39,40] Here, we report the structural engineering of layered LFS through intercalating the electron donating ET molecule in a solvothermal reaction (Table S1). The heterostructure (Li,Fe)OHFeSe ·*z*BEDT-TTF (LFS·*z*ET) induces a spin-glass-like transition which is sensitive to both the ET stoichiometry and an applied magnetic field (Table 1). A comparison of the laser-induced effects observed in the electrical transport of LFS and LFS·*z*ET heterostructures suggests the influence of charge transfer and spin interaction from ET molecules.[41]

Received: May 22, 2020
Revised: October 5, 2020
Published: October 15, 2020

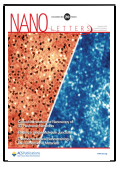

https://dx.doi.org/10.1021/acs.nanolett.0c02175
Nano Lett. 2020, 20, 7852−7859

Table 1. Chemical Structures and Magnetic Properties of van der Waals Compounds

compounds	donor	host	magnetic order	T_c (T_s)
FeSe			PM[a]	8 K
(Li,Fe)OHFeSe	(Li,Fe)OH	FeSe	PM	40 K
(Li,Fe)OHFeSe·0.0013(BEDT-TTF)	BEDT-TTF	(Li,Fe)OHFeSe	SG-like[b]	160 K
(Li,Fe)OHFeSe·0.0017(BEDT-TTF)	BEDT-TTF	(Li,Fe)OHFeSe	SG-like	145 K
(Li,Fe)OHFeSe·0.0065(BEDT-TTF)	BEDT-TTF	(Li,Fe)OHFeSe	SG-like	110 K

[a]PM: paramagnetic above superconducting critical temperature (T_c). [b]SG-like: spin-glass-like.

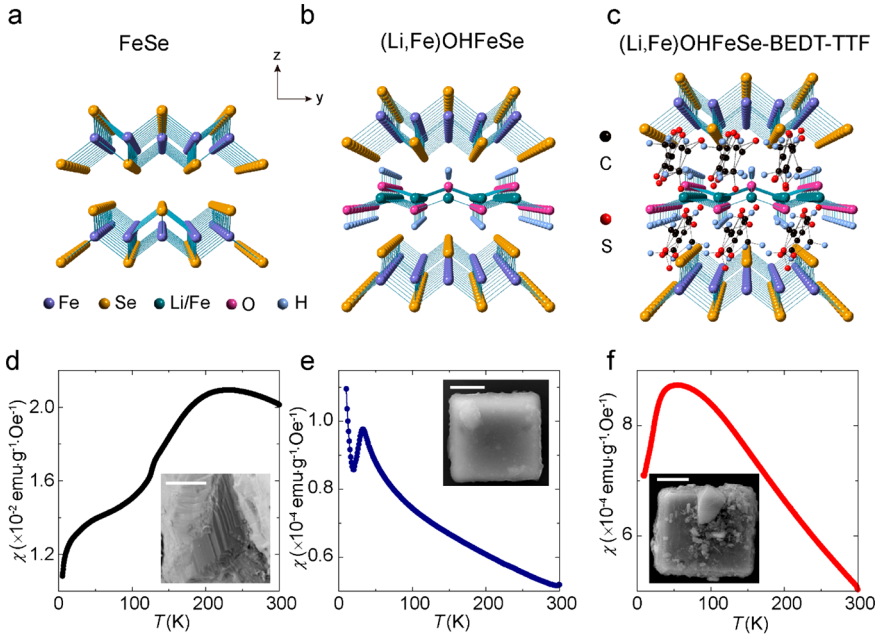

Figure 1. Crystal structures, morphologies, and magnetic susceptibilities of FeSe and its derived heterostructures. (a–c) The layered crystal structures of FeSe (FS), (Li,Fe)OHFeSe (LFS), and (Li,Fe)OHFeSe ·zBEDT-TTF (LFS-ET) illustrate the FeSe-based heterostructures engineered with LiOH and the BEDT-TTF molecule at the layer scale. The derived heterostructures inherit the layered nature of FS and are governed by van der Waals forces and hydrogen bonds. (d–f) Temperature-dependent magnetic susceptibility of FS, LFS, and LFS-ET at an applied field of 0.1 T demonstrates the large variations in magnetism that emerge as a result of molecular engineering. The scanning electron microscopic images (inset) show their surface topography and morphologic integrity that are maintained after solution reaction. The white scale bars are 1 μm in (d,f), 2 μm in (e).

The vdWs forces and hydrogen bonds play a vital role in the structural engineering of FeSe-based layered materials where organic and inorganic molecules can be intercalated into the layers to tune its electronic and spin properties.[42,43] The structure of FeSe consists of stacked and layered sheets stabilized by vdWs forces (Figure 1a). Besides, LFS shows a larger spacing between adjacent FeSe layers which are connected via hydrogen bonds with (Li,Fe)OH layers (Figure 1b).[28] The (Li,Fe)OH layer can be readily intercalated between the FeSe layers, owing to the fact that the FeSe and LiOH compounds share the common space group ($P4/nmm$) and similar tetrahedral coordination. In addition, a portion of the Li sites in the (Li,Fe)OH layer are occupied by electron donor Fe ions resulting in charge transfer to the FeSe layer and additional distribution of charges among layers.[44] Inspired by the formation of LFS heterostructure, we select electron donor ET molecule that often presents intermolecular interactions and hydrogen bonds to explore the spin-dependent and charge-transfer behavior in the LFS system. On the basis of the intercalated FeSe structures,[43,45] an LFS·zET heterostructure is schematically shown in Figure 1c. In this LFS·zET heterostructure, the ET molecule with a spatial scale of 13.33 × 3.55 × 2.55 Å^3 is an electron donor,[46,47] while sulfur and hydrogen atoms in ET molecules are inclined to form hydrogen bonds with hydrogen and selenium atoms in the (Li,Fe)OH and FeSe layers, respectively.

Magnetic susceptibilities and scanning electron microscopic images of FS, LFS, and LFS·zET reveal changes of their magnetic properties and morphology (Figure 1d–f and inset images) due to the structural engineering by intercalating electron donating molecules. Under an applied magnetic field of 0.1 T, FS shows multiple metamagnetic transitions including a broad maximum at around 200 K and a shoulder at around 130 K (Figure 1d) in addition to a diamagnetic transition below 8 K (Figure S1). The spin correlation in FS, which is characterized as an antiferromagnetic fluctuation, is likely responsible for a linear magnetic susceptibility above the low-temperature diamagnetic transition (Figure S1).[48] Molecular intercalation results in modified magnetic properties in LFS that exhibit a paramagnetic behavior (Figures 1e and S2) different from that observed in FS. In the meantime, low-temperature diamagnetic transition in FS is increased to a higher temperature that is discussed below. Specifically, the magnetic susceptibility of the LFS·zET heterostructure (Figure 1f) exhibits a broad transition at 55 K, above which the linear magnetic susceptibility dominates.

https://dx.doi.org/10.1021/acs.nanolett.0c02175
Nano Lett. 2020, 20, 7852–7859

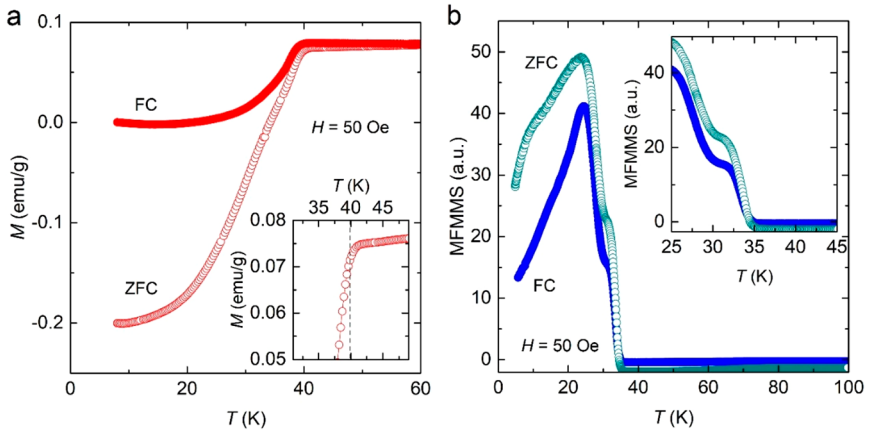

Figure 2. Superconducting properties of the LFS host material. (a) ZFC and FC diamagnetic transition at 40 K of LFS suggests a superconducting transition under an applied field at 50 Oe. (b) At the same magnetic field of 50 Oe, magnetic field-modulated microwave spectroscopy (MFMMS) confirms the onset of a superconducting transition at 35 K. Note that the 5 K difference in the value of T_c may be related to differences in thermometry between the two measurements.

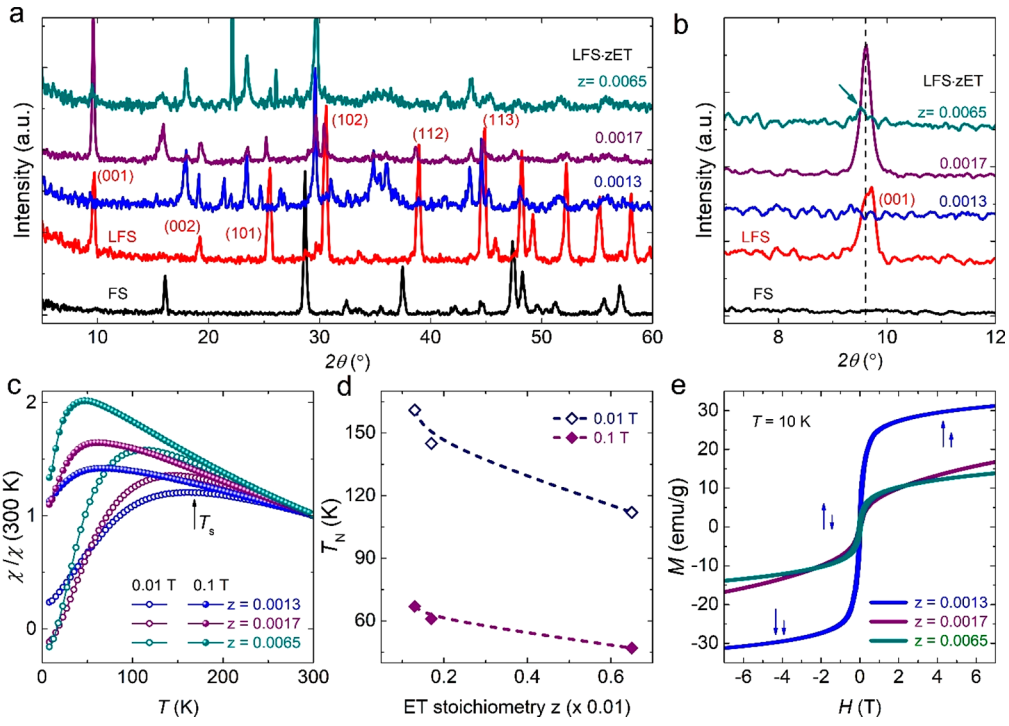

Figure 3. X-ray diffraction (XRD) patterns of FS, LFS, and LFS-ET with different stoichiometries z of ET molecules and their magnetic properties. (a) XRD patterns of FS, LFS, and LFS-ET show changes to the structure after solution reactions. (b) LFS-ET heterostructures (z = 0.0017 and 0.0065) have expanded structures that can be revealed by the slight left-shift of (001) peak compared to that of LFS. The sample of z = 0.0013 shows a vanishing (001) peak. (c) Normalized magnetic susceptibility χ/χ(300 K) show the magnetic transition. (d) The dependence of transition temperature T_s on the ET concentration z illustrates the effect of the ET molecules on the magnetism under various applied magnetic fields. (e) Magnetic field-dependent magnetization of LFS-ET heterostructures synthesized at different ET molecule concentrations shows the soft magnetic properties at 10 K.

The host material LFS for molecular interaction is superconducting, suggested from its diamagnetism and microwave spectroscopy. Figure 2a illustrates the diamagnetic transition at 40 K of the LFS powder under an applied magnetic field of 50 Oe while zero-field-cooled (ZFC) and field-cooled (FC). The inset of Figure 2a shows the ZFC diamagnetic transition near T_c = 40 K. The existence of superconductivity in the LFS powder sample is further investigated using temperature-dependent magnetic field modulated microwave spectroscopy (MFMMS). The MFMMS signals (Figure 2b) at 50 Oe (ZFC and FC) show the sharp upturns at 35 K which suggest superconductivity and corroborate the diamagnetic transition at 40 K as a superconducting transition.[49] The relatively small difference in temperature of 5 K between the onset of superconductivity in the magnetization (T_c = 40 K) and MFMMS (T_c = 35 K) measurements is not entirely understood but is possibly due to differences in thermometry.

The evolution of X-ray diffraction (XRD) patterns is shown as a function of ET stoichiometry z in the LFS·zET

https://dx.doi.org/10.1021/acs.nanolett.0c02175
Nano Lett. 2020, 20, 7852−7859

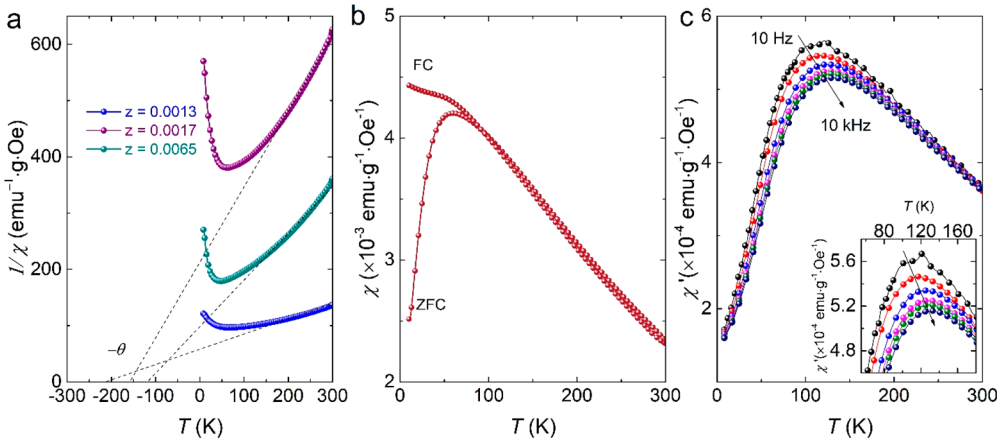

Figure 4. Spin-glass behavior with antiferromagnetic interactions in LFS·*z*ET samples. (a) Inverse magnetic susceptibilities of LFS·*z*ET samples exhibit negative intercepts ($-\theta$), suggesting antiferromagnetic interactions. (b) ZFC and FC magnetic susceptibility of LFS·*z*ET sample (z = 0.0065) at a magnetic field of 0.1 T. The irreversibility between ZFC and FC curves indicates a spin-glass-like behavior below the transition temperature. (c) Temperature-dependent real part of AC magnetic susceptibility for LFS·*z*ET sample (z = 0.0065) at frequencies of 10, 100, 1000, 3000, 5000, and 10 000 Hz. The inset shows that the transition temperature shifts to higher temperature when the frequency is increased from 10 Hz to 10 000 Hz, confirming a spin-glass state. The DC magnetic field of 100 Oe and the amplitude of 10 Oe were applied during all the AC magnetic measurements.

heterostructure to reveal the structural evolution by molecular intercalation (Figure 3a). The lattice parameters of LFS were refined as $a = b$ = 3.785 (3) Å, c = 9.333(8) Å for LFS host material (Figure S3). The (001) diffraction peak observed in the XRD pattern of LFS is observed in the LFS·*z*ET heterostructure but shifted downward, suggesting a crystal lattice expansion of the LFS·*z*ET heterostructure along *c*-axis direction after the intercalation of ET (Figure 3b). This shift to a lower angle is shown in the (001) peak for LFS·*z*ET of z = 0.0017, which is marked by the dashed line in Figure 3b. Besides, high-resolution transmission electron spectroscopy reveals the *a*-axis constant is about 3.514 Å for z = 0.0017 (Figure S4). Relative to the LFS·*z*ET heterostructure with z = 0.0017, heterostructures with higher or lower *z*-concentration exhibit XRD patterns with a weakened or nearly vanishing (001) peak. A (001) peak in LFS·*z*ET of z = 0.0065 exists and is slightly shifted to a lower angle as shown by the arrow in Figure 3b. The small (001) peak in LFS·*z*ET of z = 0.0065 and the absence of a (001) peak for LFS·*z*ET of z = 0.0013 are evidence of a change in structure and suggest that the ET intercalation occurred in the LFS·*z*ET heterostructure.[50,51] The *ab initio* calculations are applied to illustrate the intercalated structure of LFS·*z*ET heterostructure (Figure S5). The shift in peak to a lower diffraction angle occurs in each LFS·*z*ET heterostructure at different *z*-concentrations, confirming the lattice expansion upon intercalation with ET molecules. The LFS·*z*ET heterostructures present extra hexagonal coordination of the FeSe layer[52] due to the molecule intercalation, according to the Raman peak at 255 cm^{-1} (Figure S6).[52]

In contrast to the paramagnetic feature in LFS, the LFS·*z*ET heterostructure exhibits a magnetic transition, which can be tuned with either the ET stoichiometry or an applied magnetic field. Figure 3c illustrates the temperature-dependent susceptibilities of LFS·*z*ET heterostructure at different ET stoichiometries. By increasing the ET stoichiometry z from 0.0013 to 0.0065, the magnetic transition temperature T_s, defined by the location of the maximum in the magnetic susceptibility, varies from 160 to 110 K (Figure 3c). At a higher magnetic field of 0.1 T, the magnetic transition is suppressed to lower temperature, confirming the existence of magnetic-field-dependent spin coupling in LFS-ET heterostructure. In addition, when the applied magnetic field is above 0.1 T, the magnetic transition vanishes and a small upturn in the susceptibility appears (Figures S7−S9). The magnetic transition temperature T_s in LFS·*z*ET heterostructure decreases with an increase in ET stoichiometry z and also with an increase in an applied magnetic field (Figure 3d). At a fixed temperature, magnetization of LFS·*z*ET heterostructure increases rapidly with magnetic field and tends to saturate at above 1 T (Figures 3e and S10).

The magnetic state in LFS·*z*ET heterostructures is further studied as the spin-glass-like behavior and antiferromagnetic interactions. The inverse magnetic susceptibilities of LFS·*z*ET samples exhibit negative intercepts ($-\theta$), suggesting its antiferromagnetic interactions (Figure 4a). Besides, the ZFC and FC magnetic susceptibility of LFS·*z*ET heterostructure (z = 0.0065) shows an irreversibility that is often observed in a spin glass[53] (Figure 4b). Temperature-dependent AC magnetic susceptibility for LFS·*z*ET sample (z = 0.0065) at frequencies from 10 Hz to 10 kHz further confirms its spin-glass behavior (Figure 4c). The DC magnetic field of 100 Oe and the amplitude of 10 Oe are applied during the AC magnetic measurements. The inset shows that the transition temperature T_s shifts to a higher temperature when the frequency is increased, which is the representative characteristic of a spin-glass state. According to the inverse magnetic susceptibility and temperature- and frequency-dependent AC magnetic susceptibility, the spin-glass state is confirmed in LFS·*z*ET heterostructures with the predominant antiferromagnetic interactions. The *ab initio* calculations also reveal antiferromagnetic interaction in LFS·*z*ET is more energetically stable than ferromagnetic interaction (Table S2). The antiferromagnetic and ferromagnetic ground state (Figure S11a,b) have a very close energy (Table S2) so that this two states can thermally coexist like a spin glass. Intercalated ET molecules induce spin frustration that changes spin number in the preset antiferromagnetic model (Figure S11c) and involves antiferromagnetic coupling in the preset ferromagnetic model (Figure S11d). All of the *ab initio* calculations indicate the

https://dx.doi.org/10.1021/acs.nanolett.0c02175
Nano Lett. 2020, 20, 7852−7859

disordered or frustrated spin in LFS·zET which can be regarded as spin glass. Previous study on LFS system also revealed a spin-glass state at 12 K in its parent phase, nonsuperconducting and some superconducting samples,[54] even though it was claimed as a canted antiferromagnet.[28] The ET molecule in LFS·zET heterostructures seems to promote the spin-glass transition temperature through spin interaction with (Li,Fe)OH and FeSe layers.

Upon molecular intercalation of LFS with ET, the electronic transport properties of heterostructure can be affected by the electron doping from ET building blocks. Temperature-dependent electrical resistivity of LFS-ET heterostructure with ET stoichemistry z = 0.0017 shows a semiconducting behavior and a reduction in resistivity upon laser illumination (Figure 5a). After ET intercalation, the electrical resistivity ρ of

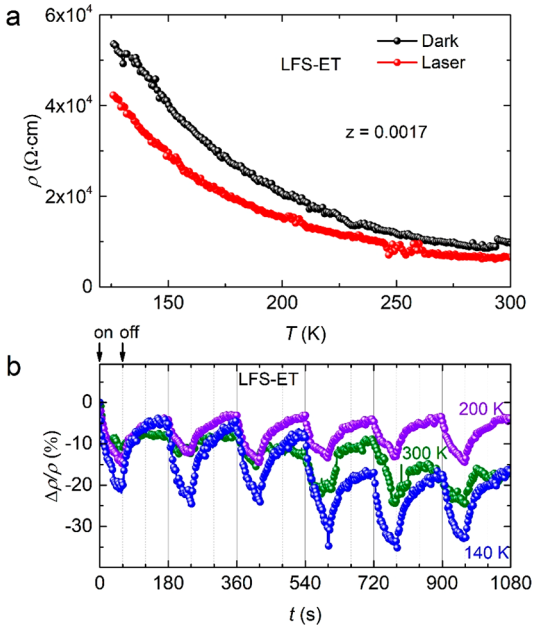

Figure 5. Laser illumination effects on electrical transport of the LFS-ET heterostructure. (a) Temperature-dependent electrical resistivity ρ of LFS-ET in the dark and under laser illumination shows the reduction in ρ. The pressed sample used for electrical measurements is shown in the inset. (b) On−off cycles of laser illumination on LFS-ET show a flexiable tunability in the relative resistivity $\Delta\rho/\rho$ = [ρ(laser) − ρ(dark)]/ρ(dark). A larger relative decrease in resistivity is found at 140 K.

LFS·zET is smaller compared to that of LFS (Figures 5a and S12 a). The reduction in electrical resistivity of LFS·zET heterostructure upon laser illumination is weaker at 300 K, which is expected, considering the divergence in the semiconducting behavior at lower temperatures. Figure 5b displays that relative electrical resistivity $\Delta\rho/\rho$ = [ρ(laser) − ρ(dark)]/ρ(dark) responses to on (60 s) and off (120 s) cycles of laser illumination at temperatures of 300, 200, and 140 K, showing the photoinduced excitation and relaxation in LFS·zET heterostructure. However, the relative decrease in resistivity $\Delta\rho/\rho$ at 140 K is larger than that of 200 and 300 K. At each temperature, the relaxation time for a complete return in the electrical resistivity is less than 120 s. Laser illumination effect on electric transport has been reported for ET-based insulators and conductors[55] due to the response of ET molecules. Besides, FeSe layer has been reported to show a higher conductivity or superconducting transition temperature by photoexcitations upon laser illumination.[56]

The multiple roles of ET molecules in LFS·zET heterostructures including electron donors and magnetic interactions might be a reason to explain the emerged spin-glass-like transition and electrical transport behavior. The ET molecules can transfer electrons into the conducting FS layers, as active electron donors,[37,38] to increase the carrier concentration and result in a decreased electrical resistivity compared to that of LFS (Figures 5a, S12, and S13) while the laser-induced thermal effect can be ruled out as the main contribution (Figures S14 and S15). Besides, the unpaired electrons in ET molecules interact with (Li,Fe)OH or FeSe layers, emerging the spin-glass-like state that is sensitive to magnetic field and ET stoichiometry. Spin glass as a certain magnetic state is spin disordered or frustrated. Regarding the antiferromagnetic interactions suggested by inverse magnetic susceptibility, LFS·zET heterostructures exist with a local spin coupling that is antiferromagnetic or canted. It seems ET molecules' intercalation transforms LFS into a spin disordered or frustrated magnet (Figure S11) due to the diluted ET concentration and fractional spin on the ET site. It could be also the reason why ET intercalation promotes the spin-glass transition at 12 K[54] in the LFS system to above 100 K. Disordered or frustrated spins can reorient along the direction of a high magnetic field, leading to the enhanced and saturated magnetization. Furthermore, two adjacent ET molecules in LFS·zET heterostructure can form dimers that can be stimulated by laser illumination,[39,57] which modifies magnetic interaction with LFS. This is consistent with the decrease of $\Delta\rho/\rho$ in a LFS·zET heterostructure near the magnetic transition temperature (Figure 5b). In addition, the structural detail and spin configuration in the LFS·zET heterostructure are still an open topic that needs further exploration for potential applications in spintronics.[58−60]

In summary, the layered superconducting material LFS has been utilized to synthesize a new heterostructure LFS·zET by intercalating with ET molecules, which play an important role on modifying magnetic interactions and electrical transport. A spin-glass-like transition emerged in the LFS·zET heterostructure at a relatively high-temperature range where the host material LFS is paramagnetic and shows a flexiable tunablility by an magnetic field and ET stochiometry. Laser illumination is a useful probe to induce free carriers and reversibly tune resistivity in LFS-ET heterostructure. The emerged magnetic transition in LFS·zET heterostructure is ascribed to interactions between FS layers and ET molecules. The reduced resistivity of LFS may originate from an increase on free carriers due to electron donation by ET molecules. The magnetic coupling and charge transfer between LFS and ET molecules provide a promising platform to study magnetism and electrical properties emerging from inorganic−organic hybrid heterostructures.

■ ASSOCIATED CONTENT

Supporting Information

The Supporting Information is available free of charge at https://pubs.acs.org/doi/10.1021/acs.nanolett.0c02175.

Materials and methods including sample preparation, structural and morphologic characterizations, magnetic susceptibility measurements, magnetic field-dependent magnetization measurements, electron transport meas-

https://dx.doi.org/10.1021/acs.nanolett.0c02175
Nano Lett. 2020, 20, 7852−7859

urements and microwave spectroscopy measurements of superconductivity; *ab initio* calculations based on density functional theory, quantitative analysis of laser-induced thermal effect (PDF)

AUTHOR INFORMATION

Corresponding Author

Shenqiang Ren − *Department of Mechanical and Aerospace Engineering, Department of Chemistry, and Research and Education in Energy, Environment, and Water (RENEW) Institute, University at Buffalo, The State University of New York, Buffalo, New York 14260, United States;* orcid.org/0000-0002-9987-3316; Email: shenren@buffalo.edu

Authors

Yulong Huang − *Department of Mechanical and Aerospace Engineering, University at Buffalo, The State University of New York, Buffalo, New York 14260, United States*

Christian Wolowiec − *Department of Physics and Center for Advanced Nanoscience, University of California San Diego, La Jolla, California 92093, United States*

Taishan Zhu − *Department of Materials Science and Engineering, Massachusetts Institute of Technology, Cambridge, Massachusetts 02139, United States*

Yong Hu − *Department of Mechanical and Aerospace Engineering, University at Buffalo, The State University of New York, Buffalo, New York 14260, United States*

Lu An − *Department of Mechanical and Aerospace Engineering, University at Buffalo, The State University of New York, Buffalo, New York 14260, United States;* orcid.org/0000-0001-9141-9365

Zheng Li − *Department of Mechanical and Aerospace Engineering, University at Buffalo, The State University of New York, Buffalo, New York 14260, United States*

Jeffrey C. Grossman − *Department of Materials Science and Engineering, Massachusetts Institute of Technology, Cambridge, Massachusetts 02139, United States;* orcid.org/0000-0003-1281-2359

Ivan K. Schuller − *Department of Physics and Center for Advanced Nanoscience, University of California San Diego, La Jolla, California 92093, United States*

Complete contact information is available at: https://pubs.acs.org/10.1021/acs.nanolett.0c02175

Author Contributions

The manuscript was written with contributions of all authors. All authors have given approval to the final version of the manuscript.

Funding

The U.S. Department of Energy, Office of Basic Energy Sciences, Division of Materials Sciences and Engineering supports S.R. under Award DE-SC0018631 (Organic conductors). Financial support was provided by the U.S. Army Research Office supports S. R. under Award W911NF-18-2-0202 (Materials-by-Design and Molecular Assembly). The superconductivity research at UCSD was supported by the AFOSR Grant FA9550-14-1-0202 and the organic aspects by the NSF-DMR-1805585.

Notes

The authors declare no competing financial interest.

REFERENCES

(1) Gaita-Arino, A.; Luis, F.; Hill, S.; Coronado, E. Molecular Spins for Quantum Computation. *Nat. Chem.* **2019**, *11*, 301−309.

(2) Wang, X.; Sun, G.; Li, N.; Chen, P. Quantum Dots Derived from Two-Dimensional Materials and Their Applications for Catalysis and Energy. *Chem. Soc. Rev.* **2016**, *45*, 2239−62.

(3) Kalb, N.; Reiserer, A. A.; Humphreys, P. C.; Bakermans, J. J. W.; Kamerling, S. J.; Nickerson, N. H.; Benjamin, S. C.; Twitchen, D. J.; Markham, M.; Hanson, R. Entanglement Distillation between Solid-State Quantum Network Nodes. *Science* **2017**, *356*, 928−932.

(4) Togan, E.; et al. Quantum Entanglement between an Optical Photon and a Solid-State Spin Qubit. *Nature* **2010**, *466*, 730−4.

(5) Wehling, T. O.; Novoselov, K. S.; Morozov, S. V.; Vdovin, E. E.; Katsnelson, M. I.; Geim, A. K.; Lichtenstein, A. I. Molecular Doping of Graphene. *Nano Lett.* **2008**, *8*, 173−7.

(6) Li, D.; Lee, K.; Wang, B. Y.; Osada, M.; Crossley, S.; Lee, H. R.; Cui, Y.; Hikita, Y.; Hwang, H. Y. Superconductivity in an Infinite-Layer Nickelate. *Nature* **2019**, *572*, 624−627.

(7) Ueno, K.; Nakamura, S.; Shimotani, H.; Yuan, H. T.; Kimura, N.; Nojima, T.; Aoki, H.; Iwasa, Y.; Kawasaki, M. Discovery of Superconductivity in $KTaO_3$ by Electrostatic Carrier Doping. *Nat. Nanotechnol.* **2011**, *6*, 408−12.

(8) Merino, P.; Svec, M.; Pinardi, A. L.; Otero, G.; Martin-Gago, J. A. Strain-Driven Moire Superstructures of Epitaxial Graphene on Transition Metal Surfaces. *ACS Nano* **2011**, *5*, 5627−34.

(9) Yanagi, K.; Kanda, S.; Oshima, Y.; Kitamura, Y.; Kawai, H.; Yamamoto, T.; Takenobu, T.; Nakai, Y.; Maniwa, Y. Tuning of the Thermoelectric Properties of One-Dimensional Material Networks by Electric Double Layer Techniques Using Ionic Liquids. *Nano Lett.* **2014**, *14*, 6437−42.

(10) Li, L. J.; O'Farrell, E. C.; Loh, K. P.; Eda, G.; Ozyilmaz, B.; Castro Neto, A. H. Controlling Many-Body States by the Electric-Field Effect in a Two-Dimensional Material. *Nature* **2016**, *529*, 185−9.

(11) de la Venta, J.; Wang, S.; Ramirez, J. G.; Schuller, I. K. Control of Magnetism across Metal to Insulator Transitions. *Appl. Phys. Lett.* **2013**, *102*, 122404.

(12) Gibert, M.; Zubko, P.; Scherwitzl, R.; Iniguez, J.; Triscone, J. M. Exchange Bias in Lanio3-$LaMnO_3$ Superlattices. *Nat. Mater.* **2012**, *11*, 195−8.

(13) Novoselov, K. S.; Mishchenko, A.; Carvalho, A.; Castro Neto, A. H. 2d Materials and Van Der Waals Heterostructures. *Science* **2016**, *353*, No. aac9439.

(14) Song, J. C. W.; Gabor, N. M. Electron Quantum Metamaterials in Van Der Waals Heterostructures. *Nat. Nanotechnol.* **2018**, *13*, 986−993.

(15) Lutchyn, R. M.; Bakkers, E. P. A. M.; Kouwenhoven, L. P.; Krogstrup, P.; Marcus, C. M.; Oreg, Y. Majorana Zero Modes in Superconductor-Semiconductor Heterostructures. *Nature Reviews Materials* **2018**, *3*, 52−68.

(16) Gong, C.; Zhang, X. Two-Dimensional Magnetic Crystals and Emergent Heterostructure Devices. *Science* **2019**, *363*, eaav4450.

(17) Liu, Y.; Huang, Y.; Duan, X. Van Der Waals Integration before and Beyond Two-Dimensional Materials. *Nature* **2019**, *567*, 323−333.

(18) Wu, J.; Liu, F.; Sasase, M.; Ienaga, K.; Obata, Y.; Yukawa, R.; Horiba, K.; Kumigashira, H.; Okuma, S.; Inoshita, T.; Hosono, H. Natural Van Der Waals Heterostructural Single Crystals with Both Magnetic and Topological Properties. *Science Advances* **2019**, *5*, eaax9989.

(19) Benitez, L. A.; Savero Torres, W.; Sierra, J. F.; Timmermans, M.; Garcia, J. H.; Roche, S.; Costache, M. V.; Valenzuela, S. O. Tunable Room-Temperature Spin Galvanic and Spin Hall Effects in Van Der Waals Heterostructures. *Nat. Mater.* **2020**, *19*, 170.

(20) Lee, D.-H. Routes to High-Temperature Superconductivity: A Lesson from Fese/Srtio3. *Annu. Rev. Condens. Matter Phys.* **2018**, *9*, 261−282.

(21) Zhao, W. W.; Li, M. D.; Chang, C. Z.; Jiang, J.; Wu, L. J.; Liu, C. X.; Moodera, J. S.; Zhu, Y. M.; Chan, M. H. W. Direct Imaging of

Electron Transfer and Its Influence on Superconducting Pairing at Fese/$SrTiO_3$ Interface. *Sci. Adv.* **2018**, *4*, No. eaao2682.
(22) Huang, S. X.; Chien, C. L.; Thampy, V.; Broholm, C. Control of Tetrahedral Coordination and Superconductivity in $FeSe_{0.5}Te_{0.5}$ Thin Films. *Phys. Rev. Lett.* **2010**, *104*, 217002.
(23) Kwon, J.; Jun, S. W.; Choi, S. I.; Mao, X.; Kim, J.; Koh, E. K.; Kim, Y.-H.; Kim, S.-K.; Hwang, D. Y.; Kim, C.-S.; Lee, J. Fese Quantum Dots for in Vivo Multiphoton Biomedical Imaging. *Sci. Adv.* **2019**, *5*, eaay0044.
(24) Song, C. L.; Zhang, H. M.; Zhong, Y.; Hu, X. P.; Ji, S. H.; Wang, L.; He, K.; Ma, X. C.; Xue, Q. K. Observation of Double-Dome Superconductivity in Potassium-Doped Fese Thin Films. *Phys. Rev. Lett.* **2016**, *116*, 157001.
(25) He, S. L.; et al. Phase Diagram and Electronic Indication of High-Temperature Superconductivity at 65 K in Single-Layer Fese Films. *Nat. Mater.* **2013**, *12*, 605−10.
(26) Ge, J.-F.; Liu, Z.-L.; Liu, C.; Gao, C.-L.; Qian, D.; Xue, Q.-K.; Liu, Y.; Jia, J.-F. Superconductivity above 100 K in Single-Layer Fese Films on Doped $SrTiO_3$. *Nat. Mater.* **2015**, *14*, 285−289.
(27) Guo, J. G.; Jin, S. F.; Wang, G.; Wang, S. C.; Zhu, K. X.; Zhou, T. T.; He, M.; Chen, X. L. Superconductivity in the Iron Selenide $K_xFe_2Se_2$ ($0 \leq X \leq 1.0$). *Phys. Rev. B* **2010**, *82*, 180520R.
(28) Lu, X. F.; et al. Coexistence of Superconductivity and Antiferromagnetism in $(Li_{0.8}Fe_{0.2})$OHFeSe. *Nat. Mater.* **2015**, *14*, 325−9.
(29) Guo, Z.; Sun, F.; Yuan, W. Chemical Intercalations in Layered Transition Metal Chalcogenides: Syntheses, Structures, and Related Properties. *Cryst. Growth Des.* **2017**, *17*, 2238−2253.
(30) Sun, J. P.; Shahi, P.; Zhou, H. X.; Huang, Y. L.; Chen, K. Y.; Wang, B. S.; Ni, S. L.; Li, N. N.; Zhang, K.; Yang, W. G.; Uwatoko, Y.; Xing, G.; Sun, J.; Singh, D. J.; Jin, K.; Zhou, F.; Zhang, G. M.; Dong, X. L.; Zhao, Z. X.; Cheng, J.-G. Reemergence of High-T_c Superconductivity in the $(Li_{1-x}Fe_x)OHFe_{1-y}Se$ under High Pressure. *Nat. Commun.* **2018**, *9*, 380.
(31) Parkin, S. S. P.; Engler, E. M.; Schumaker, R. R.; Lagier, R.; Lee, V. Y.; Scott, J. C.; Greene, R. L. Superconductivity in a New Family of Organic Conductors. *Phys. Rev. Lett.* **1983**, *50*, 270−273.
(32) Coronado, E.; Galan-Mascaros, J. R.; Gomez-Garcia, C. J.; Laukhin, V. Coexistence of Ferromagnetism and Metallic Conductivity in a Molecule-Based Layered Compound. *Nature* **2000**, *408*, 447−9.
(33) Kagawa, F.; Miyagawa, K.; Kanoda, K. Unconventional Critical Behaviour in a Quasi-Two-Dimensional Organic Conductor. *Nature* **2005**, *436*, 534−7.
(34) Muller, J.; Brandenburg, J.; Schlueter, J. A. Magnetic-Field Induced Crossover of Superconducting Percolation Regimes in the Layered Organic Mott System Kappa-$(BEDT\text{-}TTF)_2Cu[N(CN)_2]Cl$. *Phys. Rev. Lett.* **2009**, *102*, 047004.
(35) Pratt, F. L.; Baker, P. J.; Blundell, S. J.; Lancaster, T.; Ohira-Kawamura, S.; Baines, C.; Shimizu, Y.; Kanoda, K.; Watanabe, I.; Saito, G. Magnetic and Non-Magnetic Phases of a Quantum Spin Liquid. *Nature* **2011**, *471*, 612−6.
(36) Furukawa, T.; Miyagawa, K.; Taniguchi, H.; Kato, R.; Kanoda, K. Quantum Criticality of Mott Transition in Organic materials. *Nat. Phys.* **2015**, *11*, 221−224.
(37) Sato, T.; Miyagawa, K.; Kanoda, K. Electronic Crystal Growth. *Science* **2017**, *357*, 1378−1381.
(38) Hassan, N.; Cunningham, S.; Mourigal, M.; Zhilyaeva, E. I.; Torunova, S. A.; Lyubovskaya, R. N.; Schlueter, J. A.; Drichko, N. Evidence for a Quantum Dipole Liquid State in an Organic Quasi-Two-Dimensional Material. *Science* **2018**, *360*, 1101−1104.
(39) Sasaki, T.; Yoneyama, N.; Nakamura, Y.; Kobayashi, N.; Ikemoto, Y.; Moriwaki, T.; Kimura, H. Optical Probe of Carrier Doping by X-Ray Irradiation in the Organic Dimer Mott Insulator Kappa-$(BEDT\text{-}TTF)_2Cu[N(CN)_2]Cl$. *Phys. Rev. Lett.* **2008**, *101*, 206403.
(40) Toda, Y.; Mertelj, T.; Naito, T.; Mihailovic, D. Femtosecond Carrier Relaxation Dynamics and Photoinduced Phase Separation in Kappa-(Bedt-Ttf)2cu[N(Cn)2]X (X = Br, Cl). *Phys. Rev. Lett.* **2011**, *107*, 227002.
(41) Gilabert, A.; Hoffmann, A.; Medici, M. G.; Schuller, I. K. Photodoping Effects in High Critical Temperature Superconducting Films and Josephson Junctions. *J. Supercond.* **2000**, *13*, 1−20.
(42) Ying, T.; Chen, X.; Wang, G.; Jin, S.; Lai, X.; Zhou, T.; Zhang, H.; Shen, S.; Wang, W. Superconducting Phases in Potassium-Intercalated Iron Selenides. *J. Am. Chem. Soc.* **2013**, *135*, 2951−2954.
(43) Burrard-Lucas, M.; et al. Enhancement of the Superconducting Transition Temperature of Fese by Intercalation of a Molecular Spacer Layer. *Nat. Mater.* **2013**, *12*, 15−19.
(44) Sun, H. L.; et al. Soft Chemical Control of Superconductivity in Lithium Iron Selenide Hydroxides $(Li_{1-x}Fe_x)OHFe_{1-y}Se$. *Inorg. Chem.* **2015**, *54*, 1958−64.
(45) Shi, M. Z.; Wang, N. Z.; Lei, B.; Shang, C.; Meng, F. B.; Ma, L. K.; Zhang, F. X.; Kuang, D. Z.; Chen, X. H. Organic-Ion-Intercalated Fese-Based Superconductors. *Phys. Rev. Mater.* **2018**, *2*, 074801.
(46) Kobayashi, H.; Cui, H.; Kobayashi, A. Organic Metals and Superconductors Based on Bets (Bets = Bis(Ethylenedithio)-Tetraselenafulvalene). *Chem. Rev.* **2004**, *104*, 5265−88.
(47) Guionneau, P.; Chasseau, D.; Howard, J. A.; Day, P. Neutral Bis(Ethylenedithio)Tetrathiafulvalene at 100 K. *Acta Crystallogr., Sect. C: Cryst. Struct. Commun.* **2000**, *56*, 453−4.
(48) Skornyakov, S. L.; Katanin, A. A.; Anisimov, V. I. Linear-Temperature Dependence of Static Magnetic Susceptibility in Lafeaso from Dynamical Mean-Field Theory. *Phys. Rev. Lett.* **2011**, *106*, 047007.
(49) Ramirez, J. G.; Basaran, A. C.; de la Venta, J.; Pereiro, J.; Schuller, I. K. Magnetic Field Modulated Microwave Spectroscopy across Phase Transitions and the Search for New Superconductors. *Rep. Prog. Phys.* **2014**, *77*, 093902.
(50) Guo, J.; Lei, H.; Hayashi, F.; Hosono, H. Superconductivity and Phase Instability of Nh3-Free Na-Intercalated $FeSe_{1-z}Sz$. *Nat. Commun.* **2014**, *5*, 4576.
(51) Hosono, S.; Noji, T.; Hatakeda, T.; Kawamata, T.; Kato, M.; Koike, Y. New Superconducting Phase of $Li_x(C_6H_{16}N_2)_yFe_{2-z}Se_2$ with T_c = 41 K Obtained through the Post-Annealing. *J. Phys. Soc. Jpn.* **2016**, *85*, 013702.
(52) Kumar, P.; Kumar, A.; Saha, S.; Muthu, D. V. S.; Prakash, J.; Patnaik, S.; Waghmare, U. V.; Ganguli, A. K.; Sood, A. K. Anomalous Raman Scattering from Phonons and Electrons of Superconducting $FeSe_{0.82}$. *Solid State Commun.* **2010**, *150*, 557−560.
(53) Sagredo, V.; Morón, M. C.; Betancourt, L.; Delgado, G. E. Antiferromagnetic Versus Spin-Glass Like Behavior in $MnIn_2S_4$. *J. Magn. Magn. Mater.* **2007**, *312*, 294−297.
(54) Woodruff, D. N.; Schild, F.; Topping, C. V.; Cassidy, S. J.; Blandy, J. N.; Blundell, S. J.; Thompson, A. L.; Clarke, S. J. The Parent Li(OH)FeSe Phase of Lithium Iron Hydroxide Selenide Superconductors. *Inorg. Chem.* **2016**, *55*, 9886−9891.
(55) Tajima, N.; Fujisawa, J.-i.; Naka, N.; Ishihara, T.; Kato, R.; Nishio, Y.; Kajita, K. Photo-Induced Insulator-Metal Transition in an Organic Conductor A-$(BEDT\text{-}TTF)_2I_3$. *J. Phys. Soc. Jpn.* **2005**, *74*, 511−514.
(56) Yang, M.; Yan, C.; Ma, Y.; Li, L.; Cen, C. Light Induced Non-Volatile Switching of Superconductivity in Single Layer Fese on Srtio3 Substrate. *Nat. Commun.* **2019**, *10*, 85.
(57) Yoneyama, N.; Sasaki, T.; Kobayashi, N.; Furukawa, K.; Nakamura, T. X-Ray Irradiation Effect on Magnetic Properties of Dimer-Mott Insulators: K -$(BEDT\text{-}TTF)_2Cu[N(CN)_2]Cl$ and '-$(BEDT\text{-}TTF)_2ICl_2$. *Phys. B* **2010**, *405*, S244−S246.
(58) Baltz, V.; Manchon, A.; Tsoi, M.; Moriyama, T.; Ono, T.; Tserkovnyak, Y. Antiferromagnetic Spintronics. *Rev. Mod. Phys.* **2018**, *90*, 015005.
(59) Lapidus, S. H.; McConnell, A. C.; Stephens, P. W.; Miller, J. S. Structure and Magnetic Ordering of a 2-D $Mn^{II}(TCNE)I(OH_2)$ (TCNE = Tetracyanoethylene) Organic-Based Magnet (T(C) = 171 K). *Chem. Commun. (Cambridge, U. K.)* **2011**, *47*, 7602−4.

https://dx.doi.org/10.1021/acs.nanolett.0c02175
Nano Lett. 2020, 20, 7852−7859

(60) Heron, J. T.; et al. Deterministic Switching of Ferromagnetism at Room Temperature Using an Electric Field. *Nature* **2014**, *516*, 370−3.

https://dx.doi.org/10.1021/acs.nanolett.0c02175
Nano Lett. 2020, 20, 7852−7859